

# The impact of temperature fluctuations on the large scale clustering of the Ly $\alpha$ forest

Bradley Greig,<sup>1,2,3\*</sup> James S. Bolton,<sup>3,4†</sup> & J. Stuart B. Wyithe;<sup>2,3‡</sup>

<sup>1</sup>*Scuola Normale Superiore, Piazza dei Cavalieri 7, 56126 Pisa, Italy*

<sup>2</sup>*School of Physics, University of Melbourne, Parkville, Victoria 3010, Australia*

<sup>3</sup>*ARC Centre of Excellence for All-sky Astrophysics (CAASTRO)*

<sup>4</sup>*School of Physics and Astronomy, University of Nottingham, University Park, Nottingham, NG7 2RD, UK*

7 December 2024

## ABSTRACT

We develop a semi-analytic method for assessing the impact of the large scale IGM temperature fluctuations expected following He II reionization on three dimensional clustering measurements of the Ly $\alpha$  forest. Our methodology builds upon the existing large volume, mock Ly $\alpha$  forest survey simulations presented by Greig et al. (2011) by including a prescription for a spatially inhomogeneous ionising background, temperature fluctuations induced by patchy He II photoheating and the clustering of quasars. This approach enables us to achieve a dynamic range within our semi-analytic model substantially larger than currently feasible with computationally expensive, fully numerical simulations. The results agree well with existing numerical simulations, with large scale temperature fluctuations introducing a scale dependent increase in the spherically averaged 3D Ly $\alpha$  forest power spectrum of up to 20–30 per cent at wavenumbers  $k \sim 0.02 \text{ Mpc}^{-1}$ . Although these large scale thermal fluctuations will not substantially impact upon the recovery of the baryon acoustic oscillation scale from existing and forthcoming dark energy spectroscopic surveys, any complete forward modelling of the broadband term in the Ly $\alpha$  correlation function will nonetheless require their inclusion.

**Key words:** intergalactic medium - quasars: absorption lines - cosmology: theory - large scale structure of the Universe

## 1 INTRODUCTION

The Ly $\alpha$  forest is a powerful probe of large-scale structure in the intergalactic medium (IGM). It is characterised by a series of narrow absorption features imprinted into the spectra of bright background sources, and arises from the resonant scattering of Ly $\alpha$  photons by intervening neutral hydrogen (Rauch 1998). The observed transmitted flux yields information on the underlying physical properties of the IGM, such as the gas density, ionisation state and temperature, and is sensitive to the matter power spectrum at small scales,  $1\text{--}80 h^{-1} \text{ Mpc}$ , along the line-of-sight (Croft et al. 2002; Viel et al. 2004; McDonald et al. 2006; Seljak et al. 2006; Palanque-Delabrouille et al. 2013).

Recently, Busca et al. (2013) (see also Slosar et al.

2013; Font-Ribera et al. 2014; Delubac et al. 2014) reported the first successful detection of baryon acoustic oscillations (BAOs) in the Ly $\alpha$  forest from the Baryon Oscillation Spectroscopic Survey (BOSS). These observations have highlighted the potential of the Ly $\alpha$  forest for probing the *three dimensional* large-scale clustering of structure within the IGM, in addition to the existing 1D line-of-sight measurements. However, these data (as well as results from forthcoming surveys such as eBOSS and DESI) will also be sensitive to large scale fluctuations of *astrophysical* origin. Large scale variations in the ionisation and thermal state of the IGM in particular may be detectable at  $2 < z < 3$  (Slosar et al. 2009; White et al. 2010; McQuinn et al. 2011). Indeed, both Pontzen (2014) and Gontcho A Gontcho et al. (2014) have recently developed analytical models for investigating the impact of very large-scale ( $k < 0.01 h \text{ Mpc}^{-1}$ ) ionisation fluctuations on the Ly $\alpha$  forest. At the mean BOSS redshift of  $z \sim 2.3$ , these studies concluded there should be a measurable impact on the H I power spectrum at large scales

\* E-mail: b.greig@student.unimelb.edu.au (BG),

† james.bolton@nottingham.ac.uk (JSB)

‡ swyithe@unimelb.edu.au (JSBW),

as a result of the interplay between the clustering of the IGM and fluctuations in the underlying H I fraction.

However, significant fluctuations in the IGM temperature of order  $\sim 10^4$  K are also expected to linger following the reionization of singly ionised helium (He II) at  $z \sim 3$  (McQuinn et al. 2009; Compostella et al. 2013). These will result in large scale variations in the H I fraction through the temperature dependence of the H II recombination coefficient,  $\alpha_{\text{HII}} \propto T^{-0.7}$ . Gontcho A Gontcho et al. (2014) briefly discussed the impact that these temperature fluctuations might have on the Ly $\alpha$  power spectrum, although as noted by these authors, their analytic model was not suitable for fully modelling both the local and global effects of heating during He II reionization. Earlier work by McQuinn et al. (2011) also investigated the signature of temperature fluctuations in the IGM using an analytical argument combined with radiative transfer simulations of He II reionization (McQuinn et al. 2009). These authors found order of unity variations in the amplitude of the 3D Ly $\alpha$  forest power spectrum at  $k < 0.1 \text{ Mpc}^{-1}$ . However, the simulations used to perform the McQuinn et al. (2011) analysis were not large enough to sample fluctuations on scales  $\lesssim 0.05 \text{ Mpc}^{-1}$ , nor were the Ly $\alpha$  forest spectra extracted from the radiative transfer simulations able to resolve the Jeans scale at mean density. Self-consistently modelling the expected signature of temperature fluctuations in Ly $\alpha$  spectroscopic surveys is thus extremely computationally challenging. A large dynamic range is required to simultaneously resolve small-scale structure in the Ly $\alpha$  forest and probe sufficiently large cosmic volumes which incorporate the sparse ionising sources (quasars, e.g. Furlanetto & Oh 2008a) thought to drive the temperature fluctuations.

An alternative approach is therefore to use simplified but significantly more efficient techniques to investigate this problem. In this context, Greig et al. (2011) (hereafter GBW11) developed an efficient, large-volume mock Ly $\alpha$  forest survey model which was used to simulate the signature of BAOs in the Ly $\alpha$  forest. The results agreed well with a variety of observational measurements after calibration against hydrodynamical simulations, and were additionally able to sample large cosmological volumes ( $\sim 1 \text{ Gpc}^3$ ) at high resolution ( $\sim 240 \text{ kpc}$ ). In this work we now extend this model to examine the effect of temperature fluctuations following He II reionization on measurements of large-scale clustering with the Ly $\alpha$  forest.

The paper is organised as follows. In Section 2 we outline modifications made to our previous simulations and then describe our model for large scale temperature fluctuations in Section 3. We then investigate the impact of these large-scale thermal fluctuations on the Ly $\alpha$  forest in Section 4. Finally, in Section 5 we summarise our results and provide our closing remarks. Throughout this work we assume a  $\Lambda$ CDM cosmology with,  $h = 0.72$ ,  $\Omega_{\text{m}} = 0.26$ ,  $\Omega_{\Lambda} = 0.74$ ,  $\Omega_{\text{b}} = 0.0444$ ,  $n_{\text{s}} = 0.96$  and  $\sigma_8 = 0.8$ . These are equivalent to our calibration hydrodynamical simulation, model L3 of Bolton et al. (2010).

## 2 LARGE SCALE Ly $\alpha$ FOREST SIMULATIONS

Our Ly $\alpha$  models are based on the fast, large volume simulations developed by GBW11. This is itself based on a model developed by Viel et al. (2002), whereby a linear density field undergoes a rank-ordered mapping of its probability distribution to the corresponding distribution from a calibration hydrodynamical simulation. Although this model does not correctly capture the mildly non-linear structure probed by the Ly $\alpha$  forest on small scales, it is very well suited for studying the fluctuations on large scales considered here. We direct the reader to GBW11 for further discussion and tests of our Ly $\alpha$  forest model. Here we restrict ourselves to describing only the new components we have implemented for examining the effect of temperature fluctuations on Ly $\alpha$  forest clustering following He II reionization. Note that all quantitative results in this work are obtained at redshift  $z = 2.5$  using  $1 \text{ Gpc}^3$  comoving simulation volumes with  $4096^3$  pixels.

### 2.1 Clustering of ionising sources

Quasars, with their hard non-thermal spectra, are the sources considered most likely to drive the process of He II reionization (Madau et al. 1999; Furlanetto & Oh 2008a; McQuinn et al. 2009). These sources are known cluster on scales of a few tens of Mpc (Shen et al. 2007) and to be strongly biased tracers of the large-scale structure. Therefore, to develop a physically motivated model for temperature fluctuations in the IGM following He II reionization, we must first identify the location of the quasars in our simulation volume.

We achieve this by performing an iterative procedure to identify suitable locations for the ionising sources. This begins with a large ( $1 \text{ Gpc}^3$ ) volume box which contains a gridded  $4096^3$  linear IGM density field in Fourier space. This is then smoothed on a mass-scale of  $5 \times 10^{12} M_{\odot}$  by a top-hat filter in real-space, roughly corresponding to the expected characteristic halo mass hosting a luminous quasar. After Fourier transforming the density field to real space, a pixel is then flagged as a candidate quasar location when (i) its smoothed linear density exceeds four times the linear critical density for collapse and (ii) it is the highest density peak within a grid centred on the candidate pixel which extends 8 pixels from centre to edge. Finally, we sort all candidate quasar locations by their smoothed linear overdensity, sampling from highest to lowest. As a test of this procedure, we have computed the quasar correlation function recovered by this approach and verified there is excellent agreement to the observed clustering of luminous quasars presented by (Shen et al. 2007).

### 2.2 Spatial fluctuations in the ionising background

With our prescription for identifying the locations of the ionising sources in hand, we now turn to modelling the spatial fluctuations in the ionising background. We use the method outlined by Bolton & Viel (2011) for this purpose (see also Furlanetto 2009).

First, we must assign luminosities to the quasar locations identified in our simulation volume using the observed quasar luminosity function (QLF). The number of quasars to be placed within our simulation volume,  $V$ , is obtained by integrating the  $B$ -band QLF,  $\phi(L_B, z)$  of Hopkins et al. (2007),

$$N(L_B > L_{\min}) = V \int_{L_{\min}}^{\infty} \phi(L_B, z) dL_B, \quad (1)$$

where we assume a limiting magnitude of  $L_{\min} = 10^{44.25} \text{ erg s}^{-1}$  ( $M_B = -22$ ) in this work.

We next assign each quasar a  $B$ -band luminosity by Monte-Carlo sampling the observed QLF, selecting from our sorted list of candidate quasars until we obtain  $N(L_B > L_{\min})$  sources. We assume a broken power-law spectral energy distribution (Madau et al. 1999),

$$L_{\nu} = \begin{cases} \nu^{-0.3} & (2500 < \lambda < 4600 \text{ \AA}), \\ \nu^{-0.8} & (1050 < \lambda < 2500 \text{ \AA}), \\ \nu^{-\alpha_s} & (\lambda < 1050 \text{ \AA}), \end{cases} \quad (2)$$

where  $\alpha_s$  is the extreme UV (EUV) index. Telfer et al. (2002) obtained  $\alpha_s = 1.57 \pm 0.17$  from a sample of low redshift, radio quiet quasars and additionally observed significant source-to-source variations, characterised as a Gaussian distribution with a mean  $\alpha_s \approx 1.6$  and a standard deviation of 0.86. More recently, Shull et al. (2012) and Stevans et al. (2014) recovered a mean spectral index of  $\alpha_s = 1.41$  from HST-COS observations at  $z < 1.5$ . We therefore encompass the large observed variability in  $\alpha_s$  by Monte Carlo sampling a Gaussian with a mean of 1.5 and standard deviation 0.5 over the range of three standard deviations.

We next calculate  $J(\mathbf{x}, \nu)$  [ $\text{erg s}^{-1} \text{ cm}^{-2} \text{ Hz}^{-1} \text{ sr}^{-1}$ ], the specific intensity of the ionising background. For the  $N$  quasars in our simulation volume, at frequencies between the H I and He II photoionisation edges,  $\nu_{\text{HI}} < \nu < \nu_{\text{HeII}}$ , the total contribution to the ionising background is given by,

$$J(\mathbf{x}, \nu) = \frac{1}{4\pi} \sum_{i=1}^N \frac{L_i(\mathbf{x}_i, \nu)}{4\pi|\mathbf{x} - \mathbf{x}_i|^2}, \quad (3)$$

where  $|\mathbf{x} - \mathbf{x}_i|$  is the distance at a point  $\mathbf{x}$  to quasar  $i$ . We have assumed the IGM is optically thin below the He II ionisation threshold; recently reported values for the mean free path for H I ionising photons at  $z = 2.4$  are in the range  $\sim 500$ – $860$  comoving Mpc (Rudie et al. 2013; O’Meara et al. 2013), which is an appreciable fraction of our  $1 \text{ Gpc}^3$  simulation volume. As a result, our simulations do not capture the very large scale ( $k < 0.01 \text{ Mpc}^{-1}$ ) ionisation fluctuations discussed recently by Pontzen (2014) and Gontcho A Gontcho et al. (2014).

At frequencies above the He II ionisation threshold,  $\nu > \nu_{\text{HeII}}$ , the ionising background is instead,

$$J(\mathbf{x}, \nu) = \frac{1}{4\pi} \sum_{i=1}^N \frac{L_i(\mathbf{x}_i, \nu)}{4\pi|\mathbf{x} - \mathbf{x}_i|^2} e^{-\frac{|\mathbf{x} - \mathbf{x}_i|}{\lambda_{\text{HeII}}} \left(\frac{\nu}{\nu_{\text{HeII}}}\right)^{-3(\beta-1)}}, \quad (4)$$

where  $\lambda_{\text{HeII}}$  is the mean free path of ionising photons at the He II ionisation threshold, which is a highly uncertain quantity that will vary substantially during He II reionization. Models derived from the observed H I column density distribution report values in the range  $\sim 90$ –

114 Mpc at  $z = 2.5$  to  $\sim 15$ – $36$  Mpc (comoving) at  $z = 3$  (Davies & Furlanetto 2014; Khaire & Srianand 2013). In this work we assume  $\lambda_{\text{HeII}} = 45$  comoving Mpc, which is similar to the expected mean separation of luminous quasars at  $z \sim 2.5$  (Davies & Furlanetto 2014). This choice maximises the impact of temperature fluctuations on our results at  $z = 2.5$ ; larger mean free paths will result in smaller temperature fluctuations in our model. Note, however, that since the adiabatic cooling timescale in the low density IGM is long,  $t \sim H^{-1}$ , thermal fluctuations imprinted during He II reionization at  $z \sim 3$  – when the mean free path may be rather short – will also persist to lower redshift, and so the assumption of a smaller mean free path is likely reasonable (see also Gontcho A Gontcho et al. (2014)). We further approximate the column density distribution for He II absorbers in the diffuse IGM to follow a power law with  $\beta = 1.5$ . While this will broadly capture the effect of Poisson distributed absorbers on the frequency dependence of the mean free path, the distribution will start to deviate from a single power-law when H I and He II become optically thick (Fardal et al. 1998; Haardt & Madau 2012).

Finally, to calculate the specific intensity we evaluate Eq. (3) and (4) using 30 frequency bins spanning the range 1–100 Ryd. The photoionisation rates [ $\text{s}^{-1}$ ] are then

$$\Gamma_i(\mathbf{x}) = \int_{\nu_i}^{\infty} 4\pi\sigma_i(\nu)J(\mathbf{x}, \nu) \frac{d\nu}{h_{\text{p}}\nu}, \quad (5)$$

and the photoheating rates [ $\text{erg s}^{-1}$ ] are

$$g_i(\mathbf{x}) = \int_{\nu_i}^{\infty} 4\pi\sigma_i(\nu)h_{\text{p}}(\nu - \nu_i)J(\mathbf{x}, \nu) \frac{d\nu}{h_{\text{p}}\nu}. \quad (6)$$

Here, the subscript  $i$  denotes three species of hydrogen and helium (H I, He I and He II),  $h_{\text{p}}$  is Planck’s constant,  $\sigma_i(\nu)$  is the photoionisation cross-section and  $\nu_i$  is the ionisation threshold.

Assuming neutral hydrogen is in photo-ionisation equilibrium, the H I number density at any location within our simulation volume is then obtained via,

$$n_{\text{HI}}(\mathbf{x}, z) = \frac{\alpha_{\text{HeII}}(T)}{\Gamma_{\text{HI}}(\mathbf{x})} \frac{2 - Y}{2(1 - Y)} n_{\text{H}}^2(\mathbf{x}, z). \quad (7)$$

Here,  $\alpha_{\text{HeII}}(T)$  is the temperature dependent recombination rate,  $\Gamma_{\text{HI}}(\mathbf{x})$  is the spatially varying photoionisation rate determined from Equation (5) and  $Y$  is the helium mass fraction, for which we assume  $Y = 0.24$  (Planck Collaboration XVI 2014).

### 2.3 Patchy heating from He II reionization

For the final part of our semi-analytical patchy heating model, we use the above calculation of the inhomogeneous ionising background at  $E > 4 \text{ Ryd}$  to estimate the temperature of the IGM following He II reionization (see also Raskutti et al. 2012; Lidz & Malloy 2014 for related approximate approaches for heating during H I reionization at  $z > 5$ ).

During He II reionization, the excess energy of an He II ionising photon above the ionisation threshold goes into heating the IGM, resulting in a substantial boost to the overall temperature. The precise amount of heating will depend on the intrinsic spectral shape of the

ionising background and the degree of hardening as the radiation is filtered through the IGM. In practice, the excess energy per photoionisation for a power law spectrum,  $L_\nu \propto \nu^{-\alpha_s}$ , will vary between the optically thin and thick limits,  $\langle E \rangle_{\text{thin}} = h_p \nu_{\text{HeII}} / (\alpha_s + 2)$  to  $\langle E \rangle_{\text{thick}} = h_p \nu_{\text{HeII}} / (\alpha_s - 1)$  (Abel & Haehnelt 1999).

We may thus estimate the expected temperature boost in the IGM following He II reionization as (Furlanetto & Oh 2008b),

$$\Delta T(\mathbf{x}) = 0.035 f_{\text{HeII}} \left( \frac{2}{3k_B} \right) \langle E_{\text{HeII}}(\mathbf{x}) \rangle. \quad (8)$$

Here,  $\langle E_{\text{HeII}}(\mathbf{x}) \rangle = g_{\text{HeII}}(\mathbf{x}) / \Gamma_{\text{HeII}}(\mathbf{x})$  is the average excess energy per He II photoionisation (which will vary between  $\langle E_{\text{thin}} \rangle \sim 15.5 \text{ eV}$  and  $\langle E_{\text{thick}} \rangle \sim 108.8 \text{ eV}$  for  $\alpha_s = 1.5$ ) at position  $\mathbf{x}$  within our simulation volume and  $f_{\text{HeII}}$  is the He II fraction in the IGM when He II photo-heating commences (we assume  $f_{\text{HeII}} = 1$ ). This expression assumes the excess energy per He II photoionisation is shared with the baryons in the IGM via Coulomb interactions. Secondary ionisations by fast electrons will only occur  $\sim 1$  per cent of the time and can be ignored here (Shull & van Steenberg 1985; McQuinn et al. 2009).

The last step is to then add the temperature boost from Eq. (8) to an initial thermal state prior to He II reionization. We follow the procedure used in GBW11 and assume the IGM temperature follows a well defined power-law temperature density relation at  $1 + \delta \leq 10$  (e.g. Hui & Gnedin 1997), and a constant temperature at higher overdensities where radiative cooling becomes important, such that

$$T_{\text{init}} = T_0 \begin{cases} (1 + \delta_b)^{\gamma-1} & (1 + \delta_b) \leq 10 \\ 10^{\gamma-1} & (1 + \delta_b) > 10. \end{cases} \quad (9)$$

In this work we assume  $T_0 = 10\,000 \text{ K}$ , consistent with measurements of the IGM thermal state at  $z \sim 4 - 5$ , prior to the onset of He II reionization (Schaye et al. 2000; Lidz et al. 2010; Becker et al. 2011). Note, however,  $\gamma$  is still poorly constrained at these redshifts; we therefore adopt a value of  $\gamma = 1.3$  which lies in the middle of the theoretically expected range of  $\gamma = 1.0 - 1.6$ .

The IGM temperature in our patchy heating model is then computed by adding the expected temperature boost from He II photo-heating to Eq. (9),

$$T_{\text{IGM}} = T_{\text{init}} + \Delta T(\mathbf{x}). \quad (10)$$

As we shall now demonstrate in the next section, this simple, semi-analytical model allows us to qualitatively capture the effect of large scale temperature fluctuations on the Ly $\alpha$  forest without resorting to expensive radiative transfer simulations.

### 3 THERMAL FLUCTUATIONS IN THE IGM FOLLOWING He II REIONIZATION

#### 3.1 Predicted heating following He II reionization

Figure 1 displays the results of our simple model for temperature fluctuations in  $250 \text{ Mpc}^2$  slices within our simulation volume. Clockwise from top left, the panels show

the rank-ordered non-linear IGM density (see GBW11 for details), the IGM temperature following the addition of a temperature boost from He II photo-heating, the H I photoionisation rate and the magnitude of the temperature boost predicted by Eq. (8).

The first point to note is that the quasars – which reside at the positions where  $\Gamma_{\text{HI}}$  is largest in the lower right panel – clearly trace the overdense regions observed in the upper left panel, as expected. It is also evident that patchy He II photo-heating modifies the IGM temperature substantially, with fluctuations of order  $\sim 10^4 \text{ K}$  on scales of several hundred Mpc. Regions in the direct vicinity of the quasars are cooler, primarily because they are preferentially heated by softer He II ionising photons with relatively short mean free paths. Conversely, the furthest regions from the quasars are hottest as they are preferentially ionised by high energy (hard) ionising photons with long mean free paths. Qualitatively, this picture is similar to the radiative transfer (RT) simulations of McQuinn et al. (2009) and Compostella et al. (2013), who also find regions furthest from the quasars tend to be hottest following He II reionization. Note, however, that in the RT simulations, the timing of He II reionization also plays a role – regions close to quasars are ionised first and have a longer time to cool adiabatically. This effect acts in addition to the spectral filtering effect, and is not incorporated into the simple time independent implementation used here.

Quantitatively, we observe an average temperature boost of  $\approx 4\,000 \text{ K}$  in the vicinity of the quasars. Regions of the IGM furthest from the quasars instead typically achieve  $\Delta T \approx 8\,000 - 10\,000 \text{ K}$ . For comparison, McQuinn et al. (2009) find an average temperature boost at mean density of  $\approx 12\,000 \text{ K}$ , although some of the regions reionised last in their simulations experience  $\Delta T \gtrsim 30\,000 \text{ K}$ . More recent simulations from Compostella et al. (2013) find a slightly lower temperature boost at mean density of  $\approx 10\,000 \text{ K}$ . Observational measurements of the IGM temperature from the curvature of the transmitted flux in the Ly $\alpha$  forest also indicate a boost in the IGM temperature of  $\approx 8\,000 - 10\,000 \text{ K}$  (for an assumed  $\gamma = 1.3$ , Becker et al. 2011). Our simple model thus broadly reproduces the expected level of heating in the IGM following He II reionization for gas at mean density. Note, however, we do not recover the  $\Delta T \gtrsim 30\,000 \text{ K}$  heating observed in the IGM in the simulations by McQuinn et al. (2009), which is in part due to the fact we have no sub-grid prescription for the (uncertain) additional filtering of the ionising radiation by dense structures in the IGM (see e.g. Meiksin & Tittley 2012). On the other hand, as the volume filling factor of these very hot regions remains low, and the largest temperature boosts are confined to dense regions ( $1 + \delta > 10$ ) which are not well probed by the Ly $\alpha$  forest at  $z \sim 2.5$ , this is unlikely to impact significantly on our results.

#### 3.2 The temperature-density relation

Radiative transfer simulations of He II reionization also indicate that soon after the commencement of He II reionization, the IGM temperature-density relation may take

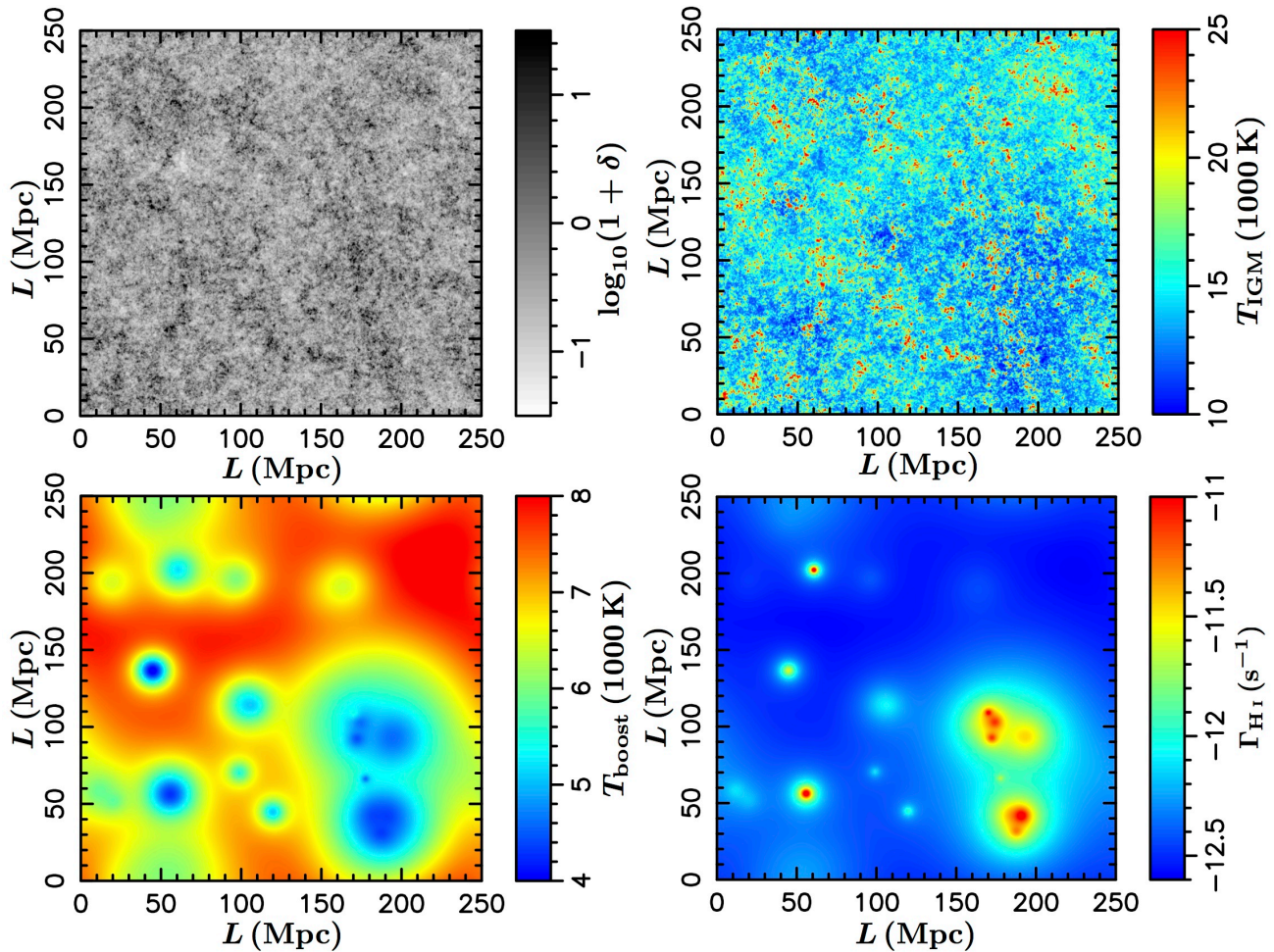


**Figure 1.** Slices through our Ly $\alpha$  forest model at  $z = 2.5$ . *Top left:* The rank-ordered IGM density contrast (see GBW11 for details). *Top right:* The IGM temperature following He II photo-heating. *Bottom left:* The boost to the IGM temperature following He II photo-heating. *Bottom right:* The H I photoionisation rate. The clustering of the ionising sources (quasars) is clearly apparent in this panel.

on a bimodal distribution (McQuinn et al. 2009; Bolton et al. 2009; Meiksin & Tittley 2012; Compostella et al. 2013). The recently photo-heated gas will tend to follow a separate temperature-density relation to the remainder of the IGM which is yet to be reionised. Following the completion of He II reionization, the bimodal IGM temperature-density relation disappears and the gas starts to cool adiabatically. However, significant scatter (in excess of that expected from optically thin models) and a shallower slope for the temperature-density relation persist.

In Figure 2, we provide an example IGM temperature-density scatter plot to demonstrate our simple model also captures this effect following He II reionization. The results of our simulation (contours and shaded region) are compared to the assumed power-law expression adopted by GBW11 (red line). The boost in the IGM temperature and the increased scatter in the relationship following He II reionization is clear on comparison to our initial temperature-density relation,  $T_{\text{init}}$  (blue line). There is furthermore very good agreement between the temperature-density relation in our semi-analytical

model and the results from the radiative transfer simulations of McQuinn et al. (2009) and Compostella et al. (2013). We find, at all IGM densities, a comparable level of scatter in the IGM temperature and similar (i.e. shallower) slope for the temperature-density relation relative to the value of  $\gamma = 1.3$  assumed prior to He II photo-heating. Overall, these results give us confidence that our simple model will capture the impact of He II photo-heating on the IGM adequately.

#### 4 THE LARGE SCALE CLUSTERING OF THE Ly $\alpha$ FOREST

In the previous sections we have outlined our semi-analytical prescription for incorporating large scale temperature fluctuations into the fast, efficient Ly $\alpha$  forest simulations developed by GBW11. We now shift our focus to investigating the impact these fluctuations may have on the Ly $\alpha$  forest, paying particular attention to their effect on the 3D Ly $\alpha$  forest power spectrum.

In what follows we consider two separate cases.

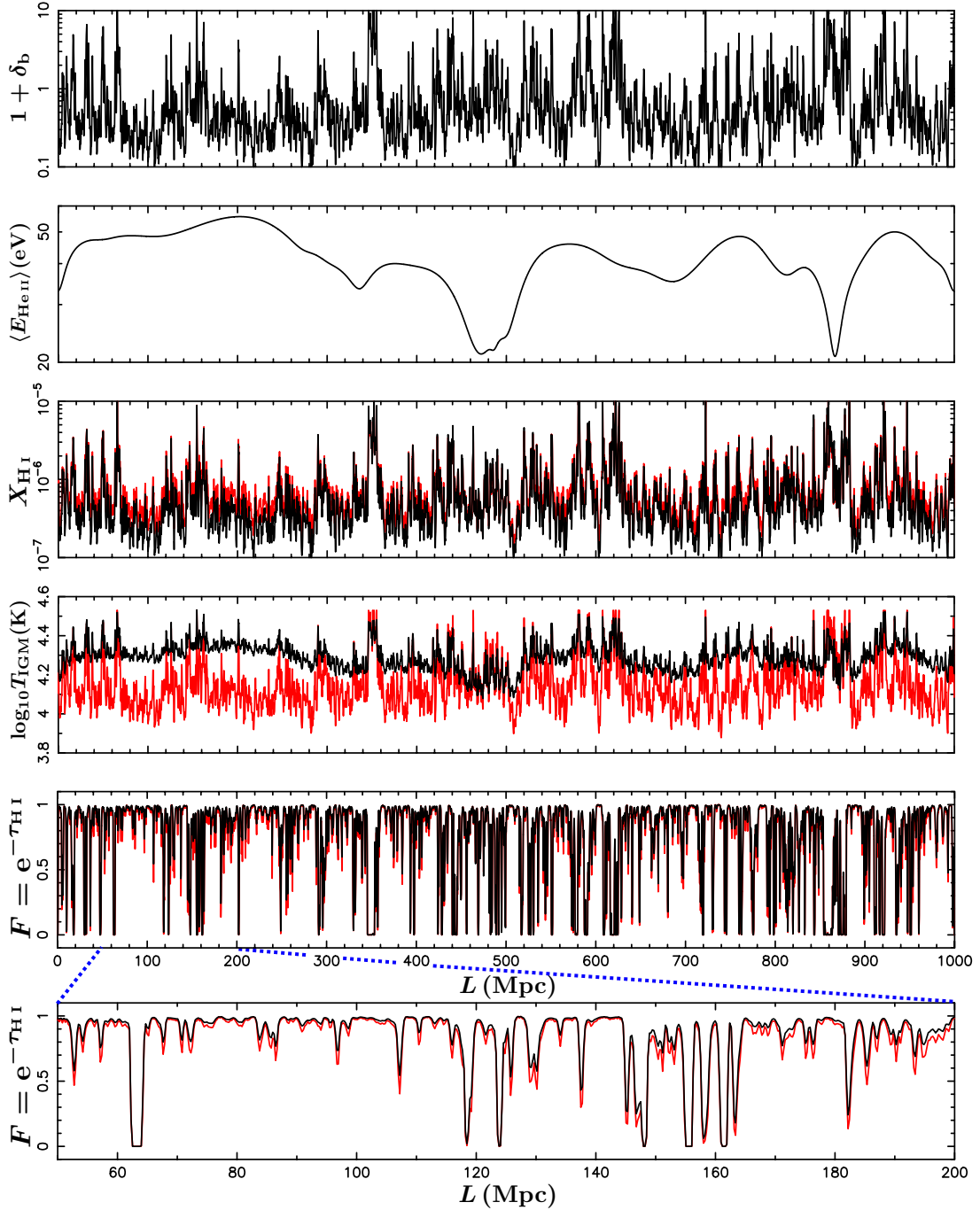


**Figure 3.** A line-of-sight drawn randomly through our  $\text{Ly}\alpha$  forest simulation. From top to bottom, the panels display: the rank-ordered IGM density contrast; the average excess energy per He II ionisation; the H I fraction  $X_{\text{HI}} = n_{\text{HI}}/n_{\text{H}}$ ; the gas temperature; the transmitted fraction  $F = e^{-\tau}$ , and a 150 Mpc zoom in of the  $\text{Ly}\alpha$  forest spectrum in the previous panel. In all panels, the black (red) curves display models including (excluding) the large scale temperature fluctuations computed using Eq. (8).

First, a model with the He II photo-heating rates implemented as described above, and second an otherwise identical model with the IGM temperature fluctuations added using Eq. (10) removed. In the latter case, we assume a single IGM temperature-density relation, with  $T_0 = 17000$  K and  $\gamma = 1.3$ . In each case we produce 10 independent realisations, enabling us to explore the box-to-box scatter in our models (i.e. cosmic variance). The method for producing  $\text{Ly}\alpha$  forest spectra from our simu-

lations remain unchanged from GBW11. After constructing our synthetic  $\text{Ly}\alpha$  forest spectra, we renormalise the pixel optical depths to match the mean observed  $\text{Ly}\alpha$  flux at  $z = 2.5$  from the high resolution sample of Faucher-Giguère et al. (2008).



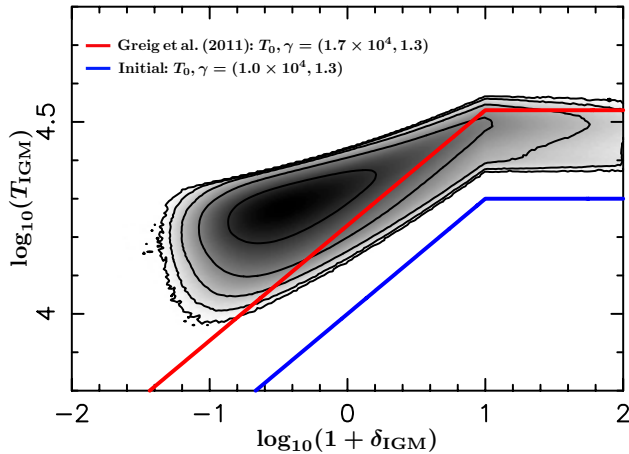


**Figure 2.** Contour plot of the temperature-density relation recovered from our Ly $\alpha$  forest model at  $z = 2.5$ . The shaded region corresponds to the normalised frequency of the data while the solid contours represent 90, 70, 50, 30 and 10 per cent of this maximal value. The blue curve corresponds to the  $T_{\text{init}}$ , while the red curve corresponds to the temperature-density relation (without inhomogeneous He II photo-heating) used by GBW11.

#### 4.1 Synthetic Ly $\alpha$ forest spectra

In Figure 3 we display a synthetic Ly $\alpha$  forest spectrum drawn through our 1 Gpc<sup>3</sup> simulation volume. In the first panel, we show the line-of-sight IGM density contrast while in the second we show the average excess energy per He II photo-ionisation. This particular line-of-sight passes nearby several quasars, with their locations corresponding to the minima where  $\langle E_{\text{HeII}} \rangle \sim 20$  eV. These minima arise due to heating close to the quasars being dominated by ionising photons near the He II ionisation edge which have shorter mean free paths. Additionally,  $\langle E_{\text{HeII}} \rangle \sim 50$ – $60$  eV furthest from the quasars, which is only a factor of two lower than the theoretical maximum value expected if every ionising photon were absorbed with equal probability, such that  $\langle E \rangle_{\text{thick}} = h_p \nu_{\text{HeII}} / (\alpha_s - 1) = 108.8$  eV (Abel & Haehnelt 1999).

In the third and fourth panels of Figure 3 we compare the H I fraction ( $X_{\text{HI}} = n_{\text{HI}}/n_{\text{H}}$ ) and IGM temperature in our two scenarios. The red curves correspond to the model without temperature fluctuations. We observe that the IGM temperature fluctuations have an important impact on the H I fraction through the temperature dependence of the H II recombination coefficient,  $\alpha_{\text{HI}} \propto T^{-0.7}$ . The largest difference between the models occurs in the regions where the mean excess energy per photo-ionisation is greatest, resulting in a decrease in the H I fraction by as much as 60 per cent. As noted earlier, the IGM temperature in our model with patchy He II photo-heating is on average systematically higher compared to a single temperature-density power law relation. Large scale (greater than a few hundred Mpc) variations result in the gas temperature, and are driven by the heating from long range, hard ionising photons.

The final two panels in Figure 3 provide a direct comparison of the transmitted fraction in the Ly $\alpha$  forest. Note that for this comparison we have not normalised the

spectra to the same effective optical depth. As expected there is less transmission overall from the the model without temperature fluctuations, although the differences are small and are only apparent on large scales. As noted by McQuinn et al. (2011), it is for this reason that detecting  $\Delta T \sim 10^4$  K temperature fluctuations from He II reionization is difficult using 1D line-of-sight Ly $\alpha$  forest statistics based on a handful of quasar spectra (see also Theuns et al. 2002; Lai et al. 2006; Lidz et al. 2010).

#### 4.2 The 3D Ly $\alpha$ forest power spectrum

Large scale temperature fluctuations are expected to have a small effect on individual Ly $\alpha$  forest spectra and on 1D line-of-sight statistics. However, in the case of the three dimensional clustering measurements from the Ly $\alpha$  forest, temperature fluctuations may be much more important (see also White et al. 2010; McQuinn et al. 2011). We thus estimate the impact of the temperature fluctuations on the large-scale clustering measurements of the Ly $\alpha$  forest by taking the ratio of the spherically averaged 3D Ly $\alpha$  forest power spectrum from our simulations with patchy He II photo-heating and a model without temperature fluctuations. Our reconstruction of the un-aliased estimate of the 3D Ly $\alpha$  forest spectrum (which arises due to the sparsely sample Ly $\alpha$  forest number density) follows the method outlined by McDonald & Eisenstein (2007) as applied in GBW11.

In this work we assess our Ly $\alpha$  forest modelling in the context of the recent BOSS observations. We therefore process our synthetic spectra to mimic the BOSS instrumental resolution by convolving the data with a Gaussian with a FWHM of  $\sim 3.63$  Å followed by a resampling onto bins of width  $\sim 1.04$  Å. We also use the nominal mean survey design parameters of BOSS, where we measure our 3D Ly $\alpha$  forest power spectra with a quasar density of  $15 \text{ deg}^{-2}$  and add S/N = 5 per pixel (Bolton et al. 2012; Dawson et al. 2013). Note also we consider line-of-sight sections of the forest corresponding to the distance between the rest frame Ly $\alpha$  and Ly $\beta$  transitions at  $z = 2.5$  (roughly  $\sim 620$  Mpc). For each of the ten realisations we performed, we then generate 60 000 lines of sight within each simulation box and randomly sample each at our prescribed line-of-sight density to recover the 3D Ly $\alpha$  forest power spectrum 100 times. In this manner we gain a good estimate of the impact of large scale temperature fluctuations within each simulation volume.

In the left panel of Figure 4 we show the median spherically averaged 3D Ly $\alpha$  forest power spectrum computed from our two scenarios. Here the model with patchy He II photo-heating is represented by the solid curve, while the model without temperature fluctuations is given by the dashed curve. Note again that to construct these data, we recover the median power spectrum across all of our 10 realisations. Therefore, these represent the median across a sample of 1 000 individual power spectra. An increase in power on scales  $k < 0.1 \text{ Mpc}^{-1}$  is evident in the model with patchy heating. The error bars show the  $1\text{-}\sigma$  Poisson errors for a single estimate of the spherically averaged 3D Ly $\alpha$  forest power spectrum. At  $k < 0.02 \text{ Mpc}^{-1}$ , the limited number of k-space bins sampled

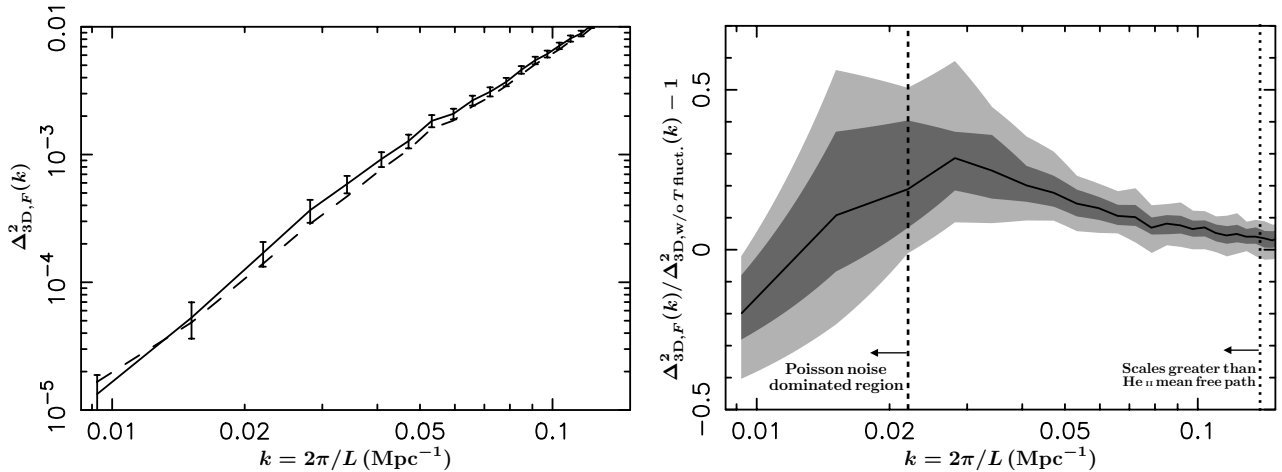


**Figure 4.** The reconstructed spherically averaged dimensionless 3D Ly $\alpha$  forest power spectra obtained from our simulations. *Left panel:* The median power spectrum from our patchy He II photo-heating model (solid curve) and our model without IGM temperature fluctuations (dashed curve). The error bars give the 1- $\sigma$  Poisson errors on the number of Fourier modes within each spherical shell in  $k$ -space. *Right panel:* The median fractional variation in the 3D power spectra obtained from our simulations. The shaded regions correspond to the predicted 68 and 95 per cent scatter around the median. Wavenumbers less than the vertical dashed line correspond to a Poisson noise dominated regime at scales approaching the box size, while wavenumbers left of the vertical dotted line denote scales greater than the mean free path at the He II ionisation edge ( $\lambda_{\text{He II}} = 45$  Mpc) assumed in our model.

at these large scales results in significant Poisson scatter which exceeds the difference between the two models (our box size corresponds to  $k = 6.2 \times 10^{-3} \text{ Mpc}^{-1}$ , and the path length between Ly $\alpha$  and Ly $\beta$  is  $k \sim 0.01 \text{ Mpc}^{-1}$ ). Our results for the 3D power spectrum at  $k < 0.02 \text{ Mpc}^{-1}$  should therefore be interpreted with caution.

Keeping this in mind, in the right panel of Figure 4 we show the fractional variation in the median spherically averaged 3D Ly $\alpha$  forest power relative to the model excluding large scale temperature fluctuations. The shaded regions correspond to the 68 and 95 per cent scatter (dark and light grey respectively) around the median fractional variance. Furthermore, the dotted line represents the wavenumber corresponding to the He II mean free path at 4 Ryd assumed in our model ( $\lambda_{\text{He II}} = 45$  Mpc). Importantly, it is only on spatial scales significantly larger than the mean free path at the ionisation edge where the temperature fluctuations have a notable impact on the large scale power. This is in part because it is the long range heating by hard photons which are responsible for producing the largest temperature (and hence H I fraction) fluctuations in our model. At spatial scales corresponding to  $k \sim 0.02 \text{ Mpc}^{-1}$  the temperature fluctuations increase large scale power up to 20-30 per cent, with the 95 per cent scatter around the median showing an increase of up to  $\sim 60$  per cent. Furthermore, this is a scale dependent effect. At decreasing spatial scales (larger  $k$ ), the amplitude of the temperature fluctuations is smaller, and the temperature fluctuations have a limited effect on the power spectrum at  $k > 0.1 \text{ Mpc}^{-1}$ . Note, however, that this inference is model dependent. In particular, if the mean free path for He II ionising photons is larger than we have assumed, or if the sources responsible for reionising He II are more numerous and/or less clustered, we expect the effect of temperature fluctuations on the

large scale power to be smaller. Our results nevertheless suggest that with detailed forward modelling of the 3D Ly $\alpha$  power spectrum, it may be possible to probe the inhomogeneous thermal state of the IGM following He II reionization with existing and forthcoming spectroscopic surveys.

In previous work, Pontzen (2014) and Gontcho A Gontcho et al. (2014) constructed analytical models that serve to illustrate the dominant contributions to variations in the H I clustering power. However, both studies focus on spatial fluctuations in the ionising background, which as discussed earlier will operate on somewhat larger scales than the temperature fluctuations considered here. Gontcho A Gontcho et al. (2014) do briefly address the potential effect of photo-heating during He II reionization, finding a rather small impact on the Ly $\alpha$  correlation function. However, these authors use the intensity of the He II ionising radiation (rather than the mean excess energy per He II ionisation) to compute the bias factor for thermal fluctuations in their model. This may not fully capture the important effect hard photons with long mean free paths have on the photo-heating rate. On the other hand, using a combination of numerical and analytical modelling McQuinn et al. (2011) observe that temperature fluctuations increase large scale power by of order unity on scales  $k < 0.1 \text{ Mpc}^{-1}$ , again suggesting that our semi-analytical model captures the effect of the temperature fluctuations reasonably well.

### 4.3 Recovery of the BAO scale

We now briefly turn our attention to the impact of large-scale IGM temperature fluctuations on the recovery of the BAO scale. A number of studies have already noted that fluctuations in the ionising background may add broad-



band power to the 3D Ly $\alpha$  forest correlation function, which could be fit and marginalised over by the addition of a smoothed component (Slosar et al. 2009; McQuinn et al. 2011; Pontzen 2014; Gontcho A Gontcho et al. 2014). In the case of strong ionising background fluctuations both Slosar et al. (2009) and Pontzen (2014) observed that these could shift the recovered BAO position by a few per cent, although this is within the noise of the BAO measurements from BOSS (Busca et al. 2013; Slosar et al. 2013; Font-Ribera et al. 2014; Delubac et al. 2014).

Consequently, to similarly assess the impact of temperature fluctuations on the recovery of the BAO scale we closely follow the approach used in GBW11. We perform two concurrent Ly $\alpha$  forest simulations, one with and one without BAOs. We then take the ratio of the 3D Ly $\alpha$  forest power spectra predicted by these two simulations, and recover an estimate of the BAO scale using a simple two parameter model. We perform this test for models including and excluding patchy He II photo-heating. In both cases, we confirm there is little impact on the recovery of the BAO scale. The large scale temperature fluctuations result only in the addition of smooth, scale-dependent increase in power that can potentially be marginalised over. Nevertheless, as the *significance* of the recovered BAO peak is often inferred relative to the null hypothesis of no BAO peak, this broadband term is important. Consequently, a complete forward modelling of the broadband term in the Ly $\alpha$  correlation function will require the incorporation of both ionising background and temperature fluctuations.

## 5 CONCLUSIONS

The recovery of the large-scale clustering of the IGM and the BAO feature from the Ly $\alpha$  forest measured by BOSS (Busca et al. 2013; Slosar et al. 2013; Font-Ribera et al. 2014; Delubac et al. 2014) provides a new avenue for precision cosmology from the Ly $\alpha$  forest at high- $z$ . In addition, the wealth of observational data also provides a unique opportunity to explore the thermal state of the IGM following the epoch of He II reionization. However, the impact of patchy He II photo-heating on the IGM is subtle, requiring detailed modelling to extract its signature from large spectroscopic data sets.

In this work we have therefore developed a semi-analytical model for investigating the impact of large-scale temperature fluctuations on the three dimensional clustering of the Ly $\alpha$  forest. Our method is built upon an existing efficient, large-volume, mock Ly $\alpha$  forest survey model developed by Greig et al. (2011). We have modified this model to include several key ingredients required for modelling the IGM following He II reionization, including quasar clustering, a spatially varying ionising background and inhomogeneous He II photo-heating.

We find our simple prescription for patchy He II photo-heating is in very good agreement with the results from recent radiative transfer simulations of He II reionization (McQuinn et al. 2009; Compostella et al. 2013). However, the dynamic range of our modelling is substantially larger than currently possible with these more

expensive, fully numerical approaches. Large scale temperature fluctuations typically produce a 20-30 per cent increase in the 3D spherically averaged Ly $\alpha$  power spectrum at  $k \sim 0.02 \text{ Mpc}^{-1}$ , although scatter arising from cosmic variance indicates this can be as large as 50-60 per cent. Importantly, we also observe this to be a scale-dependent effect with an amplitude that increases toward larger spatial scales. Furthermore, this effect is expected to occur at scales larger than both the mean quasar separation and the mean free path of He II ionising photons at the photo-electric edge. We note, however, that our results are model dependent. An increase in the mean free path for He II ionising photons, or more numerous or less clustered ionising sources will result in a reduction in the increase of large scale power. Nevertheless, with detailed forward modelling, it may be possible to probe the inhomogeneous thermal state of the IGM following He II reionization with existing and forthcoming spectroscopic surveys.

Finally, we briefly consider the potential systematic uncertainty that large-scale temperature fluctuations may have on the recovery of the BAO scale. We find that these do not substantially impact upon the recovery of the BAO scale; large scale temperature fluctuations result only in the addition of smooth, scale-dependent increase in power that can potentially be marginalised over. However, any complete forward modelling of the broadband term in the Ly $\alpha$  correlation function will ultimately require the incorporation of both ionising background (Slosar et al. 2009; White et al. 2010; Pontzen 2014; Gontcho A Gontcho et al. 2014) and large scale thermal fluctuations.

## ACKNOWLEDGMENTS

We thank Andrew Pontzen and Satya Gontcho A Gontcho for providing useful comments on a draft version of this manuscript. BG acknowledges the support of the Australian Postgraduate Award. The Centre for All-sky Astrophysics is an Australian Research Council Centre of Excellence, funded by grant CE110001020. JSB acknowledges the support of a Royal Society University Research Fellowship.

## REFERENCES

- Abel T., Haehnelt M. G., 1999, ApJ, 520, L13
- Becker G. D., Bolton J. S., Haehnelt M. G., Sargent W. L. W., 2011, MNRAS, 410, 1096
- Bolton A. S., et al., 2012, AJ, 144, 144
- Bolton J. S., Becker G. D., Wyithe J. S. B., Haehnelt M. G., Sargent W. L. W., 2010, MNRAS, 406, 612
- Bolton J. S., Oh S. P., Furlanetto S. R., 2009, MNRAS, 395, 736
- Bolton J. S., Viel M., 2011, MNRAS, 414, 241
- Busca N. G., et al., 2013, A&A, 552, 96
- Compostella M., Cantalupo S., Porciani C., 2013, MNRAS, 435, 3169
- Croft R. A. C., Weinberg D. H., Bolte M., Burles S.,

- Hernquist L., Katz N., Kirkman D., Tytler D., 2002, *ApJ*, 581, 20
- Davies F. B., Furlanetto S. R., 2014, *MNRAS*, 437, 1141
- Dawson K. S., et al., 2013, *AJ*, 145, 10
- Delubac T., et al., 2014, *arXiv:1405.7405*
- Fardal M. A., Giroux M. L., Shull J. M., 1998, *AJ*, 115, 2206
- Faucher-Giguère C.-A., Prochaska J. X., Lidz A., Hernquist L., Zaldarriaga M., 2008, *ApJ*, 681, 831
- Font-Ribera A., et al., 2014, *JCAP*, 5, 27
- Furlanetto S. R., 2009, *ApJ*, 703, 702
- Furlanetto S. R., Oh S. P., 2008a, *ApJ*, 681, 1
- , 2008b, *ApJ*, 682, 14
- Gontcho A Gontcho S., Miralda-Escudé J., Busca N. G., 2014, *MNRAS*, 442, 187
- Greig B., Bolton J. S., Wyithe J. S. B., 2011, *MNRAS*, 418, 1980
- Haardt F., Madau P., 2012, *ApJ*, 746, 125
- Hopkins P. F., Richards G. T., Hernquist L., 2007, *ApJ*, 654, 731
- Hui L., Gnedin N. Y., 1997, *MNRAS*, 292, 27
- Khaire V., Srianand R., 2013, *MNRAS*, 431, L53
- Lai K., Lidz A., Hernquist L., Zaldarriaga M., 2006, *ApJ*, 644, 61
- Lidz A., Faucher-Giguère C.-A., Dall’Aglio A., McQuinn M., Fechner C., Zaldarriaga M., Hernquist L., Dutta S., 2010, *ApJ*, 718, 199
- Lidz A., Malloy M., 2014, *ApJ*, 788, 175
- Madau P., Haardt F., Rees M. J., 1999, *ApJ*, 514, 648
- McDonald P., Eisenstein D. J., 2007, *Phys. Rev. D*, 76, 063009
- McDonald P., et al., 2006, *ApJS*, 163, 80
- McQuinn M., Hernquist L., Lidz A., Zaldarriaga M., 2011, *MNRAS*, 415, 977
- McQuinn M., Lidz A., Zaldarriaga M., Hernquist L., Hopkins P. F., Dutta S., Faucher-Giguère C.-A., 2009, *ApJ*, 694, 842
- Meiksin A., Tittley E. R., 2012, *MNRAS*, 423, 7
- O’Meara J. M., Prochaska J. X., Worseck G., Chen H.-W., Madau P., 2013, *ApJ*, 765, 137
- Palanque-Delabrouille N., et al., 2013, *A&A*, 559, A85
- Planck Collaboration XVI, 2014, *A&A*, 571, A16
- Pontzen A., 2014, *Phys. Rev. D*, 89, 083010
- Raskutti S., Bolton J. S., Wyithe J. S. B., Becker G. D., 2012, *MNRAS*, 421, 1969
- Rauch M., 1998, *ARA&A*, 36, 267
- Rudie G. C., Steidel C. C., Shapley A. E., Pettini M., 2013, *ApJ*, 769, 146
- Schaye J., Theuns T., Rauch M., Efstathiou G., Sargent W. L. W., 2000, *MNRAS*, 318, 817
- Seljak U., Slosar A., McDonald P., 2006, *JCAP*, 10, 014
- Shen Y., et al., 2007, *AJ*, 133, 2222
- Shull J. M., Stevans M., Danforth C. W., 2012, *ApJ*, 752, 162
- Shull J. M., van Steenberg M. E., 1985, *ApJ*, 298, 268
- Slosar A., Ho S., White M., Louis T., 2009, *JCAP*, 10, 019
- Slosar A., et al., 2013, *JCAP*, 04, 026
- Stevans M. L., Shull J. M., Danforth C. W., Tilton E. M., 2014, *ApJ*, 794, 75
- Telfer R. C., Zheng W., Kriss G. A., Davidsen A. F., 2002, *ApJ*, 565, 773
- Theuns T., and T.-S. Kim S. Z., Tzanavaris P., Carswell R. F., 2002, *MNRAS*, 332, 367
- Viel M., Haehnelt M. G., Springel V., 2004, *MNRAS*, 354, 684
- Viel M., Matarrese S., Mo H. J., Theuns T., Haehnelt M. G., 2002, *MNRAS*, 336, 685
- White M., Pope A., Carlson J., Heitmann K., Habib S., Fasel P., Daniel D., Lukic Z., 2010, *ApJ*, 713, 383